Proceedings of the 2019 IEEE/ASME
International Conference on Advanced Intelligent Mechatronics
Hong Kong, China, July 8-12, 2019

Design and Optimization of a Wave Driven Solar Tracker for Floating Photovoltaic Plants*

Ruoyu Xu[2], Chongfeng Liu[2], Hengli Liu[2], Zhenglong Sun[2], Tin Lun Lam[2], and Huihuan Qian[1,2,†]

***Abstract*— With advances in the ocean exploration, Floating Photovoltaic (FPV) system becomes appealing with the advantages of less valuable land use and higher efficiency. In current development, the PV module of the system is either fixed at an angle or actuated by motor to adjust the angle for solar tracking. In this paper, a novel Tracking-type FPV (TFPV) system is proposed and analysed. Rather than using motor as the actuation method, the proposed system utilized the natural wave energy to adjust the angle of the PV module for solar tracking.**

With this design, a floating PV plant can be built with reduced total cost and increased energy harvesting efficiency. The novel solar tracking design concept and a corresponding control strategy were firstly presented. Based on its dynamic modeling, the design of the system was analysed and optimized in the aspect of the structure scheme, panel size, and the adjustment frequency. A prototype was built to verify the control strategy on a 3D motion platform to simulate the wave and wind effects.

I. Introduction

Solar energy is considered to be one of the most promising energy alternative due to its ubiquity and sustainability [1]. The most common application for the use of solar energy is the Photovoltaic (PV) systems [2]. And the noticeable rise in the electricity demand, fast depletion of fossil fuels, and environmental concerns throughout the world have led to the demand of commissioning solar PV plants in large scale. However, most large-scale deployments of PV system are located over the valuable land [3] and have a potentially significant land consumption because the installation of PV systems requires large areas [4].

This limitation can be overcome by the implementation of floating PV systems on the available water surface such as the surface of the water treatment pond replaces the conventional ground-mounted solar plants [5]. Floating PV systems have attracted more attention from both a research point of view and a market perspective due to the direct and indirect benefits related to their installation. For instance, the floating PV capacity reached 211 MWp with only considering the top 70 floating PV installations worldwide in 2018 [6]. On one hand, it is land saving [7] by using the available water surface; on the other hand, it is more effective by utilizing the reflection of light from water [8] and cooling effect of water [9], [10] . It is reported that it can also improve the water quality due to reduce the photosynthetic and algae growth [1] . Therefore, this floating PV system for energy harvesting is now being deployed in projects across the world.

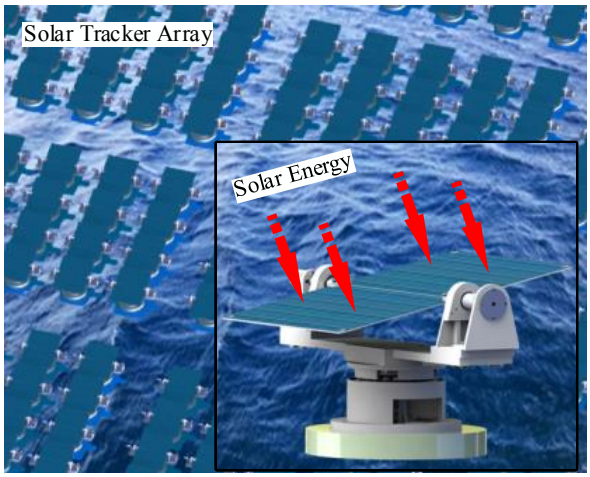

Fig. 1. Tracking-type Floating PV systems. Utilizing the wave energy to adjust the attitude of the PV module, this solar tracker is designed to harvest solar energy in ocean environment which can be applied in floating solar plants.

Floating PV system can be divided into fixed-type where the PV module is mounted at a fixed value, and tracking-type where the direction of PV module is actuated to track the sun to ensure the maximum harvesting efficiency by having the sunbeams incident perpendicularly to the PV module. Generally, it is known that, according to previous research, 20% to 50% (depending on seasons and the geographic location) increase in solar energy harvest efficiency can be achieved compared with those fixed PV systems on ground [11]. Similarly, tracking-type floating PV (TFPV) systems can achieve higher electricity production as compared to fixed-type floating PV systems. It had also been recommended that solar trackers are adopted with large PV arrays because the energy consumption of the driving systems was much less than the energy increase delivered by solar trackers [12]–[14].

Several solutions have been proposed and patented for the TFPV system [3], [15], [16]. The first TFPV system was installed in Italy in 2010, followed by the project at Lake Colignola in 2011 [15]. Terra Moretti et al. designed and constructed the TFPV system that rotated the system according to the suns direction at Petra Winery, Italy [5]. Cazzaniga et al. presented and tested an unrestricted tracking-type floating solution which consisted of a floating platform, a submersible concrete anchor and a mooring chain. The rotation was guaranteed through a sun-tracking algorithm that

*This paper is partially supported by the Shenzhen Institute of Artificial Intelligence and Robotics for Society, Project U1613226 and U1813217 from National Natural Science Foundation of China, and Robotic Discipline Development Fund (2016-1418) from Shenzhen Gov.

[1]Shenzhen Institute of Artificial Intelligence and Robotics for Society.
[2]The Chinese University of Hong Kong, Shenzhen.
[†]Corresponding author is Huihuan Qian, email: hhqian@cuhk.edu.cn

drove submerged propellers [3]. There are some other studies focusing on the structure design [16]. Nevertheless, they mostly focus on the "floating" system optimization rather than the "tracking" system, by emphasizing on the material selection and economic benefit. Also, in the literature review, it can be easily seen that most of the systems have only one DoF to track the sun, which means they cannot guarantee that the PV module is always perpendicular to the sunlight.

As shown in Fig. 1, this paper proposes a dual-axis active solar tracker as an inseparable part of TFPV system for ocean application. The device is able to track the sun automatically with the help of the wave energy which is inexhaustible in ocean environment. By substituting the motors with brakes, the cost of the whole device is decreased and the PV panels' attitude can be fixed whenever the power is cut off. The structure of the system is designed for the convenience of fabrication and assembly. In the remainder of the paper, the complete development method of the proposed solar tracker will be provided as follows:

(1) The formulation of the control algorithm which is based on the dynamic model of the proposed system.
(2) The structure design of the system which includes the determination of the PV panel position, PV panel size selection and additional weight selection. Dynamic performance is designed to satisfy specific demand.
(3) A series of experiments which test the feasibility of the control algorithms and verify the designed dynamic performance under specific fluctuation.

II. System Modelling and Control

The proposed solar tracker system has two DoFs as shown in Fig. 2. It is capable of rotating from 0° to 360° and tilting from -135° to -45°. The PV panels, whose attitude can be known via two encoders, are released or engaged by controlling the states of the brakes. The brakes are able to engage the spindle and turntable in power-off state and provide a torque which means the attitude of the PV panels can be fixed without energy consuming. In the upper part of this system, the PV panels are fixed on spindles by screws. By designing the size of the PV panels, the gravity center can be adjusted along the vertical direction of their rotation axis. Two deep groove ball bearings are mounted in the holders to support the spindles and provide one DoF rotation. The encoder and the brake are respectively mounted and fixed on one side of the spindles. In the bottom of the system, a thrust bearing is mounted to provide the other DoF rotation. The turntable, brake and encoder are mounted and connected in series to save the space. The brake is fixed on the base which ensures that the thrust bearing cannot be easily taken apart. The gravity center of the turntable can also be adjusted via additional weight. The structure has been designed for easy fabrication and assembly. In Fig. 3, the attitude of the PV panels can be easily acquired by the feedback from sensors which are given in Equation (1) and (2).

$$\zeta = \zeta_b + \gamma \tag{1}$$

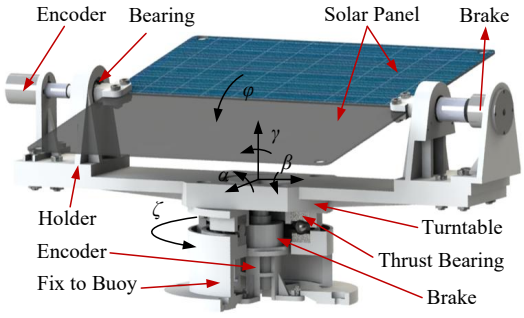

Fig. 2. CAD model of the wave driven solar tracker.

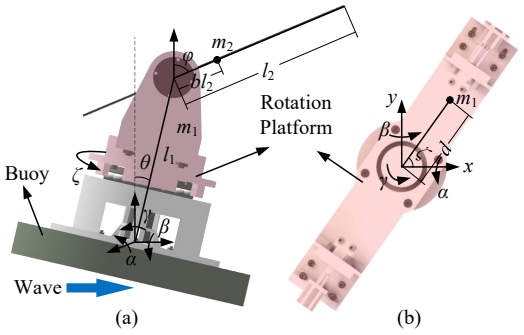

Fig. 3. Dynamic analysis. (a) The upper part of the proposed system. (b) The bottom part of the proposed system.

$$\varphi = \varphi_b + \theta \tag{2}$$

where ζ and φ are the attitude angle of the PV panel, ζ_b and φ_b are the relative rotation which can be measured by encoders. γ is the yaw of the platform which can be measured by IMU and θ is the tilting angle.

As shown in Fig. 3, the system can be seen as two parts to make it easier for dynamic model formulation. One is the rotation platform which has one DoF. Assuming the friction and the inertia of the rotation platform is constant, the dynamic model is illustrated in Fig. 3(b) which can be expressed as Equation (3).

$$M\ddot{\zeta} + M_{m1} - T_{g1} - T_{f1} = 0 \tag{3}$$

In this equation,

$$\begin{aligned} M &= I_1 + m_1 d^2,\ T_{g1} = -m_1 d g C_\beta S_\alpha C_{\zeta_d} \\ M_{m1} &= m_1 d\left(\ddot{y} C_\zeta - \ddot{x} S_\zeta\right) \end{aligned} \tag{4}$$

where C and S denote the cosine and sine operation, m_1 and I_1 are the mass and the inertia of the rotation platform, d is the eccentric distance of the rotation platform, g is the gravitational acceleration, T_{f1} is friction torque related to the thrust bearing, T_{g1} is the gravity term and α, β are the attitude angle from IMU, M and M_{m1} are inertia coefficients related to angular acceleration $\ddot{\zeta}$ and acceleration ($\ddot{x}$, $\ddot{y}$).

The other one is the upper part as shown in Fig. 3(a). It can be seen as a double inverted pendulum when looked into the structure along the rotation axis of PV panel. So the dynamic model can be expressed as Equation (5).

$$\mathbf{M}\ddot{\mathbf{q}} + \mathbf{C}(\mathbf{q}, \dot{\mathbf{q}})\dot{\mathbf{q}} + M_{m2} - T_{g2} - T_{f2} = 0 \tag{5}$$

In this equation,

$$\begin{aligned}
&\mathbf{M} = \begin{bmatrix} m_2 b l_1 l_2 C_{\varphi-\theta} \\ I_2 + b^2 m_2 l_2^2 \end{bmatrix}^{\mathrm{T}}, M_{m2} = m_2 b l_1 l_2 f(\ddot{x}, \ddot{y}, \ddot{z}) \\
&\mathbf{C}(\mathbf{q}, \dot{\mathbf{q}}) = m_2 b l_1 l_2 \dot{\theta} \begin{bmatrix} S_{\varphi-\theta} \\ 0 \end{bmatrix}^{\mathrm{T}}, \mathbf{q} = \begin{bmatrix} \theta \\ \varphi \end{bmatrix} \\
&T_{\mathrm{g2}} = b m_2 g_2 (\alpha, \beta, \zeta_{\mathrm{b}}) l_2 S_\varphi
\end{aligned} \tag{6}$$

where b denotes the position of gravity center, m_2 and I_2 are the mass and the inertia of the PV panel, T_{f2} is friction torque related to the deep groove ball bearings, g_2 is a component of the gravitational acceleration which is perpendicular to the rotational axis of the PV panel, M_{m2} is inertia coefficient related to the motion of the gravity center and θ is related to the attitude of the system base which can be deduced as Equation (7).

$$\theta = \arctan\left(\frac{S_\beta S_{\zeta_b} + C_\beta S_\alpha C_{\zeta_b}}{C_\beta C_\alpha}\right) \tag{7}$$

Assuming the nearshore wave is relatively gentle. Therefore, adjusting the attitude of the PV panels is equivalent to adjusting the elevation angle φ_{b} and azimuth angle ζ_{b} between the PV panels and the system base which is also the output of the two encoders. Assuming the motion acceleration of the system will not be very large. Substituting Equation (1) and (2) into Equation (3), (4), (5), (6), the dynamic model can be rewritten as Equation (8), (9).

$$\ddot{\zeta}_{\mathrm{b}} = -\ddot{\gamma} + \left(T_{f1} + T_{g1}\right)/M \tag{8}$$

$$\ddot{\varphi}_{\mathrm{b}} = \left(-\left(M_1 + M_2\right)\ddot{\theta} - C_1\dot{\theta} + T_{g2} + T_{f2}\right)/M_2 \tag{9}$$

where M_1 and M_2 denote the first and second element of the vector $\mathbf{M}$ and C_1 denotes the first element of $\mathbf{C}$. The control law can be expressed as Equation (10).

$$L_q = \begin{cases} \text{Release}, & \ddot{q}_b \mathrm{sign}(q_d - q_b) > \delta_1 \\ \text{Engage}, & |\dot{q}_b| < \delta_2 \end{cases} \tag{10}$$

where q_b denotes the attitude angle φ_{b} or ζ_{b}, q_d is the desired angle, $\ddot{q}_b$ can be calculated via (8) and (9) where the acceleration input can be estimated by phase looked loop. δ_1 and δ_2 are positive values which can be fine-tuned in order to tolerant the disturbance and dynamic error.

III. Structure Design

A. Gravity Center Determination for PV Panel

The value of $b \in [0, 1]$ determines the position of the PV panel. $b \neq 0$ means the PV panel is mounted eccentrically. According to Equation (8), (9) and (10), the feasibility of the PV panel control depends on the difficulty of traversing the surface $\ddot{\varphi}_{\mathrm{b}} = 0$. Obviously, the feasibility of the control law largely is determined by the value of b. In this section, a simulated wave is given and the feasibility of the control law for different b is evaluated.

Assuming the condition in one dimension, the waves period and amplitude will not change in short time and its effect on the solar tracker can be expressed by Equation (11).

$$\theta = 5\sin(5t) \tag{11}$$

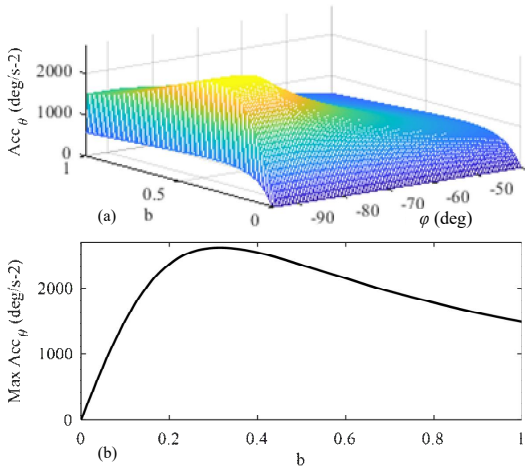

Fig. 4. Maximum demanded angular acceleration under specific fluctuation. (a) The relationship between b, ϕ and $\ddot{\theta}$. (b) maximum demanded $\ddot{\theta}$ related to different b values.

According to Equation (11), the angular velocity and acceleration of the base satisfies $\dot{\theta} \in [-25, 25]$, $\ddot{\theta} \in [-125, 125]$. In order to evaluate the feasibility of the PV panel control, the equation $\ddot{\varphi}(\varphi_b, \ddot{\theta}, \dot{\theta}, \theta, b) = 0$ needs to be solved and the maximum $\ddot{\theta}$ with respect to all the possible value of $\varphi_b, \dot{\theta}, \theta$ and b needs to be found. Here $\varphi_b \in [-90, -45]$, which is half of its range of rotation, leads to $\varphi \in [-95, -40]$ in the effect of fluctuation expressed in (11). By substituting each value of $\varphi_b, \dot{\theta}, \theta$ and b, $\ddot{\theta}$ can be solved. The maximum $\ddot{\theta}$ when b and φ equal to specific values are selected to reveal the worst possible conditions need to be satisfied. The results of $\ddot{\theta}$ are shown in Fig. 4(a). It can be seen that the maximum possible $\ddot{\theta}$ is not simple positive correlated to b. The maximum in Fig. 4(a) occurs when b is around 0.3. It is because b exists in both numerator and denominator of (9). At the same time, the figure reveals that in most combinations of b and φ, the maximum possible $\ddot{\theta}$ for traversing the surface is too huge to be satisfied by the fluctuation given in (11). The maximum values for each b in Fig. 4(a) are shown in Fig. 4(b), considering that the maximum $\ddot{\theta}$ can be provide is 125 deg/s^2, the value of b should be less than 0.01 in this condition, that will have no much difference to choose b as 0. Actually, if $b = 0$, the effect of gravity is eliminated and the inertia torque only needs to beat the frictions which is much smaller than the effect of gravity. What's more, the control law will only be related to $\ddot{\theta}$ which significantly reduces the complexity of the control algorithm.

B. The Selection of Panel Size and Additional Weight

The structure adjustment of the proposed solar tracker includes the determination of the PV panel size and the additional weight on turntable. By structure adjustment, the dynamic performance of the solar tracker can be estimated which provides a reference for the design of the system. Here fluctuation expressed in (11) is provided and the rotation angle in one period can be estimated. The process is given as follows. First, when the brake is engaged, q_{b} is invariable

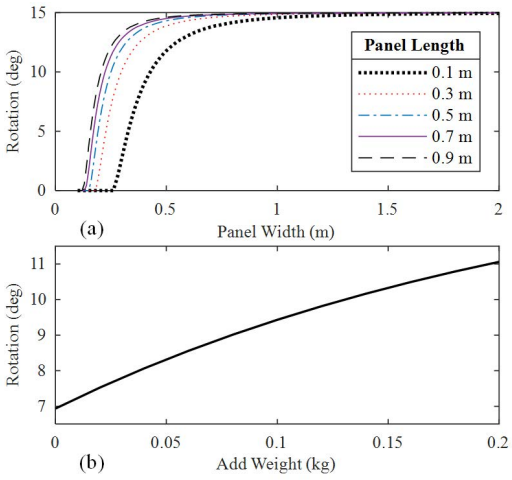

Fig. 5. Rotation angle in a period of wave. (a) The relationship between rotation angle and panel sizes. (b) The relationship between rotation angle and additional weight.

and $\dot{q}_\mathrm{b}$ is zero. When the desired position is given, the brake will be released depending on the result of (10). At the same time, $\ddot{q}_\mathrm{b}$ can be calculated by Equation (8) and (9). At last, the rotation angle in one period of fluctuation can be acquired by a simple double integral.

In the control law given in Equation (10), the value of friction does not need to be very precise because the dynamic error can be compensated by adjusting the value of δ_1 and δ_2 which also decrease the complexity of algorithms. In this section, in order to make a more accurate work, the models of friction are given as Equation (12) and (13) which can be found in the datasheets of the bearings.

$$T_{f1} = R_1 d_{\mathrm{m1}}^{1.83} F_\mathrm{l}^{0.54} \left(10\dot{\zeta}_\mathrm{b}/\pi\right)^{0.6} + 0.15 S_1 d_{\mathrm{m1}}^{0.05} F_\mathrm{l}^{1.33} + T_{fe} \quad (12)$$

$$T_{f2} = R_2 d_{\mathrm{m2}}^{1.96} F_2^{0.54} (10\dot{\varphi}_\mathrm{b}/\pi)^{0.6} + 0.15 S_2 d_{\mathrm{m2}}^{-0.26} F_2^{1.67} + T_{fe} \quad (13)$$

where F_1 and F_2 are the loads on bearing, R_1, R_2, S_1 and S_2 are parameters depends on the type of the bearings which can be acquired from their specifications. Here T_{f1} includes the thrust bearings friction where R_1 and S_1 are 1.03e-9 and 1.6e-5 respectively and T_{f2} includes the deep groove ball bearings friction where R_2 and S_2 are 4.1e-10 and 3.7e-6 respectively. d_{m1} and d_{m2} are the average diameter of bearing whose unit is millimeter and T_{fe} is the friction from encoder. By checking the specification of the encoder, the value of is T_{fe} determined as 0.001 Nm.

The simulation results are shown in Fig. 5(a) and Fig. 5(b). Figure 5(a) shows the relationship between rotation angle and panel sizes. Here the length along the rotation axis of the solar panel is defined as the panel length. It is obvious that there is a starting torque in the proposed system which constrains the minimum size of the solar panel. The panel's rotation can be more swift by enlarging its size. However, the effect will be less evident as the size is enlarged to a degree. Here the length and width will be chosen as 275 mm and 342 mm. The estimated rotation angle in one period of fluctuation is 11.37°.

Figure (5b) denotes the relationship between the turntable rotation angle and its additional weight. The rotation angle is also estimated in one period of wave. The additional weight is chosen as 0.12 kg to make the turntable and the solar panel have the similar rotation angle.

C. Times of Adjustment Decision

The frequency of attitude adjustment is optimized in this section. Solar panel adjusts its attitude automatically via waves. Adjusting the attitude of solar panel can ensure the maximum energy harvest efficiency. Solar panel system harvests most energy when it works in real time. However, adjustment operation leads to energy cost. Sometimes, brake consumes more energy than solar panel earned if it is adjusted frequently. Here, the energy consumed by brake and earned by solar panel are weighted and optimized to achieve the maximum energy profits. The energy profits can be expressed by $E_s - E_b$, where E_s is energy earned by solar panel and E_b is energy consumed by brake. Our goal is to maximize the energy efficiency which is formulated by Equation (14).

$$\max_N (E_s - E_b) \quad (14)$$

where

$$\begin{aligned}
&E_\mathrm{s} = \sum_{n=0}^{N-1} \left(\int_0^T \eta(t) E_\mathrm{m}(nT+t) t dt \right) \\
&E_\mathrm{b} = N P_\mathrm{b} t_\mathrm{b} \\
&T = T_D / N \\
&\eta(t) = \cos(\Delta\theta) \\
&\Delta\theta = \left[{\theta_\mathrm{ev}}^{nT+t} - {\theta_\mathrm{ev}}^{nT} \right] \otimes \left[{\theta_\mathrm{az}}^{nT+t} - {\theta_\mathrm{az}}^{nT} \right]
\end{aligned}$$

where N is the number of times to adjust PV panel in day time, T is the interval of adjustment, $\eta(t)$ is the harvest efficiency, T_D is the daylight duration, P_b is the rated power of brake and t_b is the average time of adjustment which can be acquired by simulation, $\otimes$ is a special operation sign defined by Equation (15).

$$A \otimes B = \arccos(cosAcosB) \quad (15)$$

$E_\mathrm{m}(t)$ is the maximum harvest power at a local time according to [17], and the solar beam irradiance is related to θ_ev, so $E_\mathrm{m}(t)$ can be calculated by Equation (16).

$$E_\mathrm{m}(t) = P_\mathrm{s} E_\mathrm{o}^n \cos(90 - \theta_\mathrm{ev}) \quad (16)$$

where P_s is the maximum power of the solar panel in a day which can be acquired by its specification. E_o^n is the eccentricity correction factor of the Earth's orbit which approximately equals to one. θ_ev and θ_az are the elevation angle and azimuth angle of the solar incident ray which are defined by Equation (17).

$$[\theta_\mathrm{ev}, \theta_\mathrm{az}] = \Theta(Lat, Lng, LT, n) \quad (17)$$

where Lat is latitude and Lng is longitude, LT is local time and n is the number of days in a year.

Take the 350^{th} day of a year for example. Assuming the location is Shenzhen, Fig. 6 is acquired by formulas above. In this condition, maximum energy profits of 76 Wh can be

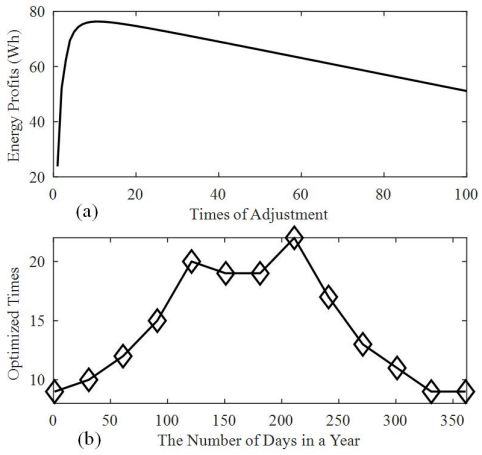

Fig. 6. (a) Simulation results under different times of adjustments. (b) Optimized times of adjustments of each day during a year.

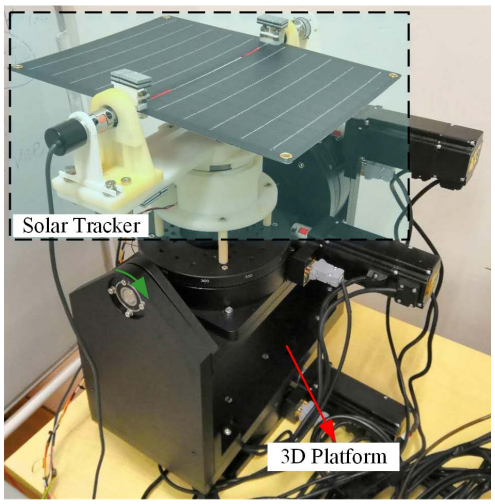

Fig. 7. Experimental prototype based on a wave-generation 3D platform.

achieved by 12 times of adjusting. That means the PV panel only needs to be adjusted once per hour to meet the best energy harvest performance.

IV. Experiment

In this section, a prototype of the solar tracker system proposed in section II is introduced. Based on the simulated wave produced by a 3D rotation platform, dynamic model of the system is verified and feasibility of the control strategy is tested.

A. Prototype

As shown in the Fig. 7, the prototype of proposed solar energy harvest system has two DoFs. The device is 450mm in length and 160mm in width. Depends on the attitude of the PV panel, the maximum height of the device is 300 mm. two 41600 mm^2 PV panels are mounted symmetrically and two ribbed plates are affixed on the backside of the panels to ensure their planeness. Considering it will not withstand too much loads, most parts of the mechanical structure are fabricated by 3D printing. The prototype weighs 2.4 kg.

TABLE I
Components and Properties

Units	Properties
Brake	Supply: 24 V, Power: 9 W, Torque: 1 Nm
Encoder	Supply: 5 V, Resolution: 0.72 deg
IMU	Supply: 5 V, Resolution: 7.6e-3 deg/s
PV Panel	Maximum Power: 7 W (14 W in total)
Total Weight:	2.4 kg (Base: 0.5 kg, Rotation Platform: 1.9 kg)

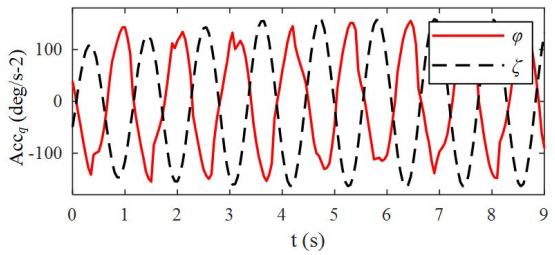

Fig. 8. The angular acceleration of φ and ζ after releasing the brakes estimated in realtime.

The hardware design of the system leads to a considerable reduction on cost. Comparing with the expensive motor used in traditional device for the same purpose, a brake costs much less. What's more, the attitude of the PV panel can be maintained without power supply while some motors need to be powered all the time or an additional brake must be applied. Table I shows the parameters of each parts applied in the prototype.

B. Attitude Control with 1-Dimension Fluctuation

The control algorithms and the dynamic performance mentioned in Section III-B are tested in this section. The fluctuation in Equation (11) can be generated by the 3D platform whose rotation can be measured by IMU. The two encoders give attitude feedback every 20 ms. The controller executes algorithms every 50 ms which includes phase locked loop for angular acceleration estimation and attitude control law. The PV panel is 342 mm in width and 275 mm in length which is mounted symmetrically. The additional weight is stuck to one side of the turntable for adjustment. The experimental results are shown in Fig. 8 and Fig. 9. The initial attitude of the PV panel is (40°, -90°) and the generated wave is supposed to drive the solar panel to the desired attitude (0°, -130°).

Figure 8 is the output of Equation (8) and (9) which is the input of the control law. Because the difference between the desired attitude and the measured attitude is positive, according to the control law (10), the PV panel will only be adjusted when the acceleration is positive too. Figure 9 shows the total rotary angle in two dimensions, the rotation in blue region is the process of adjusting ζ_b and the white region denotes the φ_b adjustment. It can be seen that the proposed solar tracker is able to adjust 80° within 9 seconds and the final error is 0.72°. The PV panel adjust once in a period of the wave and the adjusted angle in one period is around 10° which is according with the design mentioned

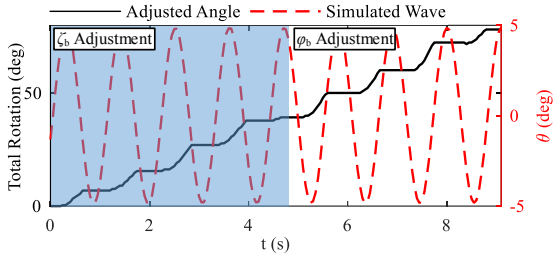

Fig. 9. Experimental result of attitude adjustment under the effect of 1D fluctuation. Black solid line denotes total rotation angle and red dotted line denotes generated wave.

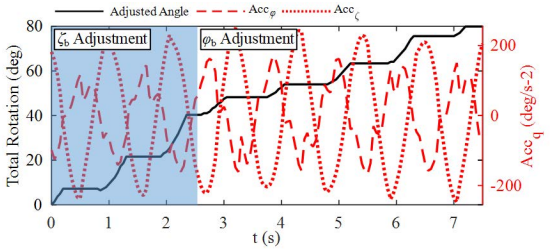

Fig. 10. Experimental result of attitude adjustment under the effect of 2D fluctuation. Black solid line denotes total rotation angle and red dotted lines denote angular accelerations after the brakes are released.

in Section III-B.

C. Attitude Control with 2-Dimension Fluctuation

The solar tracker system may experience the rotation in multi-dimension due to the effects from the coupling of waves and wind. In this section, 2D fluctuation is provided by the 3D platform to simulate more complex condition. The wave expressed by (11) is given to both yaw and tilt. The experimental results are shown in Fig. 10. The adjusted rotation angle and additional weight is the same as the 1D experiment. It can be seen that the estimated angular acceleration in yaw is bigger than that in tilt which is different from the 1D experiment. Due to the acceleration difference after releasing the brake, ζ_b takes only 2.5 seconds to adjust while φ_b takes 5 seconds to adjust itself to the desired angle. Actually, according to Equation (8) and (9), the rotation in yaw can only impact the adjustment of ζ_b. That is why φ_b takes the similar time for adjustment as 1D experiment.

V. CONCLUSION

A novel solar tracker for the TFPV system is proposed in this paper. Based on the established dynamic model and the control algorithms, the proposed solar tracker is able to adjust its attitude passively using the simulated wave motion underneath. The experiment shows that the proposed solar tracker is able to adjust 80° within 9 seconds under the effect of simulated 1D wave and the system keeps working when the fluctuation is added in both yaw and tilt. Guidelines in the system design and factors affecting the overall performance have been discussed; results are presented and verified in both simulations and experiments.

In such manner, not only can the proposed TFPV system harvest the solar energy at higher efficiency, but also it can utilise the wave energy to automatically adjust the attitude of the system. And without mechanical actuation components such as the motors, it will greatly reduce the total manufacturing and maintenance cost of a large scale floating power plant. In the next phase, a system that contains multiple PV panels will be built and evaluated in the real outdoor environment, to quantitatively assess the improvement of the energy harvesting efficiency.

REFERENCES

[1] A. Sahu, N. Yadav, and K. Sudhakar, "Floating photovoltaic power plant: A review," *Renewable and sustainable energy reviews*, vol. 66, pp. 815–824, 2016.

[2] M. Rahman, M. Hasanuzzaman, and N. Rahim, "Effects of various parameters on pv-module power and efficiency," *Energy Conversion and Management*, vol. 103, pp. 348–358, 2015.

[3] R. Cazzaniga, M. Cicu, M. Rosa-Clot, P. Rosa-Clot, G. Tina, and C. Ventura, "Floating photovoltaic plants: Performance analysis and design solutions," *Renewable and Sustainable Energy Reviews*, vol. 81, pp. 1730–1741, 2018.

[4] S. Ong, C. Campbell, P. Denholm, R. Margolis, and G. Heath, "Land-use requirements for solar power plants in the united states," National Renewable Energy Lab.(NREL), Golden, CO (United States), Tech. Rep., 2013.

[5] P. E. Campana, L. Wästhage, W. Nookuea, Y. Tan, and J. Yan, "Optimization and assessment of floating and floating-tracking pv systems integrated in on-and off-grid hybrid energy systems," *Solar Energy*, vol. 177, pp. 782–795, 2019.

[6] "Solarplaza top 70 floating solar pv plants," https://www.solarplaza.com/channels/top-10s/11761/top-70-/, (Accessed on 03/07/2019).

[7] K. Trapani, D. L. Millar, and H. C. Smith, "Novel offshore application of photovoltaics in comparison to conventional marine renewable energy technologies," *Renewable Energy*, vol. 50, pp. 879–888, 2013.

[8] Y.-K. Choi, "A study on power generation analysis of floating pv system considering environmental impact," *International journal of software engineering and its applications*, vol. 8, no. 1, pp. 75–84, 2014.

[9] T. Tsoutsos, N. Frantzeskaki, and V. Gekas, "Environmental impacts from the solar energy technologies," *Energy Policy*, vol. 33, no. 3, pp. 289–296, 2005.

[10] P. Dash and N. Gupta, "Effect of temperature on power output from different commercially available photovoltaic modules," *International Journal of Engineering Research and Applications*, vol. 5, no. 1, pp. 148–151, 2015.

[11] G. Quesada, L. Guillon, D. R. Rousse, M. Mehrtash, Y. Dutil, and P.-L. Paradis, "Tracking strategy for photovoltaic solar systems in high latitudes," *Energy conversion and Management*, vol. 103, pp. 147–156, 2015.

[12] J. Y. Muhammad, M. T. Jimoh, I. B. Kyari, M. A. Gele, and I. Musa, "A review on solar tracking system: A technique of solar power output enhancement," *Engineering Science*, vol. 4, no. 1, pp. 1–11, 2019.

[13] S. J. Oh, J. H. Hyun, Y. J. Lee, K. Chen, N. K. Choon, Y. S. Lee, and W. Chun, "A study on the development of high accuracy solar tracking systems," in *8thrwa International Conference on Sustainable energy Technologies*, 2009.

[14] J. Patil, J. Nayak, and V. Sundersingh, "Design, fabrication and preliminary testing of a two-axes solar tracking system," *International Energy Journal*, vol. 19, no. 1, 2007.

[15] Y.-K. Choi, N.-H. Lee, A.-K. Lee, and K.-J. Kim, "A study on major design elements of tracking-type floating photovoltaic systems," *International Journal of Smart Grid and Clean Energy*, vol. 3, no. 1, pp. 70–74, 2014.

[16] Y. Choi, I. Kim, S. Hong, and H. Lee, "A study on development of azimuth angle tracking algorithm for tracking-type floating photovoltaic system," *Adv. Sci. Technol. Lett*, vol. 51, no. 45, pp. 197–202, 2014.

[17] L. Wong and W. Chow, "Solar radiation model," *Applied Energy*, vol. 69, no. 3, pp. 191–224, 2001.